Polymer Chemistry

PAPER

View Article Online
View Journal | View Issue

Cite this: *Polym. Chem.*, 2014, **5**, 1945

Self-healing metallo-supramolecular polymers from a ligand macromolecule synthesized *via* copper-catalyzed azide–alkyne cycloaddition and thiol–ene double "click" reactions†

Bo Yang,[ab] Huan Zhang,[a] Huiying Peng,[a] Yuanze Xu,[a] Bowei Wu,[a] Wengui Weng*[a] and Lei Li[ab]

Received 22nd July 2013
Accepted 20th October 2013

DOI: 10.1039/c3py00975k

www.rsc.org/polymers

In this study, we develop a series of new materials that can simultaneously and reversibly self-heal without external stimuli based on metallo-supramolecular interactions. Multiple tridentate 2,6-bis(1,2,3-trizaol-4-yl)-pyridine (BTP) ligand units synthesized *via* a copper-catalyzed azide–alkyne cycloaddition (CuAAC) "click" reaction are incorporated into the polymer backbone of a ligand macromolecule through a thiol–ene "click" reaction. 3D transient supramolecular networks are formed from the ligand macromolecule upon coordination with transition and/or lanthanide metal ions. As compared to the ligand macromolecule, the resultant supramolecular films exhibit improved mechanical properties, such as Young's modulus, strength and toughness, which can be readily tuned by the stoichiometric ratio of Zn^{2+} to Eu^{3+} to Tb^{3+}. The supramolecular films exhibit characteristics of weakly crosslinked networks where the storage modulus G' and loss modulus G'' scaled with normalized frequency ωa_T by the same slope of 0.5. Both the supramolecular bulk films and gels are found to exhibit fast and effective self-healing properties by virtue of the kinetically labile nature of the metal–ligand interactions.

Introduction

Self-healing, which refers to the ability to recover an original set of properties after damage, is one of the most striking features of biological systems. Self-healing materials are expected to exhibit the advantages of improved durability, enhanced safety and prolonged lifetime of service. The last decade has witnessed a rapid development in exerting such features into artificial systems that can sense environmental changes and repair themselves accordingly.[1–9] In 2002, a milestone work was reported by White *et al.* where reactive agents were encapsulated in the matrix and subsequently released and polymerized *in situ* to repair mechanical damage.[10] Some other approaches have been developed, including hollow glass fibers,[11] solvent encapsulation,[12] 3D microvascular networks,[13,14] magnetic and electrical heating[15,16] and coaxial electrospinning.[17] Of most of the methods listed above, the repair was irreversible and involved relatively complex systems. More recently, Tang and coworkers developed hyperbranched polymers through metal-free "click" polymerizations of bis(aroylacetylene)s and triazides and demonstrated that the films and sticks made of the polymers exhibited very interesting irreversible but repeatable self-healing.[18] By taking advantage of the remaining reactive arylacetylene and azide groups on the peripheries of the polymers, the healing could be simply triggered by heating, without catalyst or other added substances.

On the other side, reversible self-healing systems based on dynamic covalent chemistry and non-covalent interactions[19–21] open new routes towards constructing more interesting self-healing materials that are capable of repetitive mending in virtue of their reversible nature. Examples in view of dynamic covalent bonds have been exploited through the use of Diels–Alder reactions,[22–25] [2 + 2] cycloadditions,[26] alkoxyamine bonds,[27] hydrazone bonds,[28] disulphide bonds,[29,30] trithiocarbonate units,[31] and olefin metathesis.[32,33] The responsiveness of these dynamic covalent bonds to external stimuli, such as temperature, pH, light and oxidants, impart the resultant materials with repetitive self-healing properties. Non-covalent interactions, including hydrogen bonding,[34–36] hydrophobic associations,[37] π–π stacking,[38–40] ionomers,[41–43] metal–ligand interactions[44–47] and host–guest interactions[48] and/or their orthogonal combinations,[49] have also been demonstrated to be successful in constructing self-healing materials.

In the case of autonomic healing without external stimuli, not only the sufficient lability of the dynamic covalent bonds

[a]*Department of Chemistry, College of Chemistry and Chemical Engineering, Xiamen University, Xiamen 361005, P. R. China. E-mail: wgweng@xmu.edu.cn*

[b]*Department of Materials Science and Engineering, College of Materials, Xiamen University, Xiamen 361005, P. R. China*

† Electronic supplementary information (ESI) available: Synthesis of BTP ligand **4**, stress–strain curves, SAXS, WAXD, rheological test and fluorescence results. See DOI: 10.1039/c3py00975k

and the supramolecular interactions, but also the sufficient mobility of the polymer chains (or oligomers) must be ensured. Of particular note are the works reported by the Leibler and Guan groups. In 2008, Leibler and co-workers demonstrated the room temperature self-healing of a supramolecular rubber which consisted of fatty acids and diethylene diamine functionalized with urea.[35] When a sample was cut into pieces and the pieces were brought into contact at 20 °C, the mobile oligomers diffused across the fracture surfaces to allow self-healing. Guan and his co-workers reported an appealing multiphase design of autonomic self-healing thermoplastic elastomers where pendent polyacrylate amide (PA-amide) chains were grafted to the backbone of polystyrene and formed dynamic molecular velcro through hydrogen-bonding in the soft phase.[50] The unleashed molecular velcro upon external loading could quickly reform under room temperature with the release of the stress owing to the low T_g of the PA-amide.

We recently used dihydroxyl functionalized tridentate 2,6-bis(1,2,3-triazol-4-yl)pyridine (BTP) ligand synthesized *via* CuAAC "click" chemistry as a chain extender to react with bis-isocyanate functionalized polytetrahydrofuran (PTHF) based prepolymer and a novel ligand macromolecule carrying multiple BTP units on the polymer backbone was synthesized which formed multi-responsive self-healing supramolecular gels in the presence of transition and/or lanthanide metal salts.[51] Although the polyurethane reaction is effective, it is moisture sensitive and may involve side reactions which can result in irreversible crosslinking. Thiol–ene chemistry appears as a new useful and versatile "click" reaction, which is moisture and oxygen insensitive and can be performed both under photochemical and thermal initiations.[52] Thus, in the present contribution, we are interested in studying the use of thiol–ene "click" chemistry in synthesizing BTP carrying a ligand macromolecule and the metallo-supramolecular gels and bulk films made of the ligand macromolecule together with metal ions.

Results and discussion

Ligand macromolecule and metallo-supramolecular polymers

The ligand macromolecule with $M_n = 12\,000$ g mol^{-1} and $M_w = 22\,000$ g mol^{-1} (Fig. 1 and S13 to S16†) was synthesized using the UV initiated thiol–ene "click" reaction of bis-propene functionalized BTP ligands and bis-thiol functionalized PTHF linkers (see ESI Schemes S1 and S2, Fig. S1 to S18†). Since the M_n of the PTHF segment is around 2000 g mol^{-1}, 5 BTP ligands were incorporated on average into the backbone of a single ligand macromolecule. The transition and lanthanide metal ions selected, *i.e.*, Zn^{2+}, Eu^{3+} and Tb^{3+}, can coordinate well with the BTP ligand to form kinetically labile 1 : 2 (Zn^{2+}) and 1 : 3 (Eu^{3+} and Tb^{3+}) metal : ligand complexes, respectively. Upon addition of metal salts into a solution of the ligand macromolecule in suitable solvents, gels can be readily formed as a result of the supramolecular crosslinking and aggregation. Clean solid films with a uniform thickness of about 0.5 mm could be harvested by casting the gels in Teflon casters and ensuing drying in a vacuum. These solid films could be reswollen in neutral solvent to take the shape of organic gels,

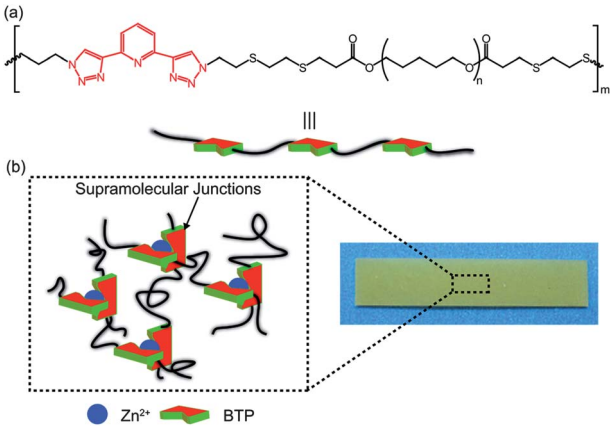

Fig. 1 (a) Multiple BTP ligand units (represented as bricks) were incorporated into the backbone of the ligand macromolecule by using bis-thiol functionalized polytetrahydrofuran (PTHF) linker (represented as black lines). (b) Bottom left: the BTP ligand units in the ligand macromolecule coordinate with metal ions (represented as balls) to form 3D transient supramolecular networks; Bottom right: a representative Zn^{2+} containing film (100:0:0).

which also exhibit multiple responsiveness and self-healing (*vide infra*). Samples are labelled in the form of *k*:*l*:*m*, where *k*, *l* and *m* denote the ideal molar percentages of the BTP ligands that bind to Zn^{2+}, Eu^{3+} and Tb^{3+}, respectively. For instance, 0:100:0 represents the BTP ligands that bind to Eu^{3+} and 0:0:0 denotes the control sample *solely* made of the ligand macromolecule. Fig. 1 shows a schematic illustration of the formation of the transient and reversible 3D supramolecular networks using the ligand macromolecule and metal ions (*e.g.*, Zn^{2+}) and one representative film of 100:0:0.

Tensile properties of the metallo-supramolecular polymers

All metal ion containing films were non-tacky under room temperature. Their key mechanical properties were first

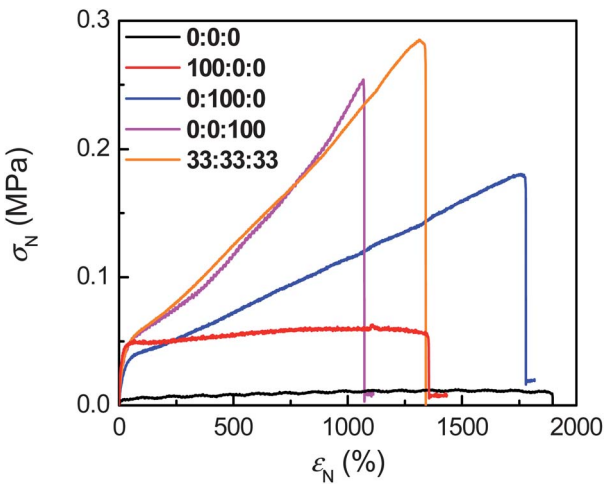

Fig. 2 Stress–strain responses of the control sample (0:0:0) and the metallo-supramolecular films containing different types of metal ions (100:0:0, 0:100:0 and 0:0:100) as well as their mixture (33:33:33).

investigated by tensile testing under a constant strain rate ($0.1\ s^{-1}$) and are depicted in Fig. 2 together with those of the control sample 0:0:0 in terms of the nominal stress σ_N as a function of the nominal strain ε_N. The control sample was quite tacky under room temperature as the glass transition temperature T_g of the PTHF segments is below room temperature. It thus showed poor mechanical properties, *e.g.*, a small Young's modulus (~4 kPa), low mechanical strength (~11 kPa) and behaved like a viscoelastic liquid during stretching. The formation of 3D transient networks by the metal–ligand supramolecular interactions significantly improved the mechanical properties of the materials. Among the three samples each containing a single type of metal ion, typical plastic deformation, *i.e.*, an almost constant nominal stress right after the yield point until fracture was observed in 100:0:0, whereas 0:100:0 and 0:0:100 showed typical elastic responses (sigmoid stress–strain shape). This difference in the mechanical properties is probably due to their different coordination numbers (2 for Zn^{2+}, 3 for both Eu^{3+} and Tb^{3+}) and morphological structures, *e.g.*, microphase separation (*vide infra*). The four parameters: tensile modulus, strength, fracture strain and toughness (total area under the tensile curves) are summarized in Table 1. Interestingly, each sample is in the lead of one typical mechanical parameter. Zn^{2+} containing films unfold the largest tensile modulus (227 ± 18 kPa) at small strain (<40%, also see Fig. S19 in the ESI†), while Eu^{3+} containing films can tolerate more extension (1800 ± 120%) than the other two and the fracture strain is very close to the control sample (1700 ± 325%). For a given value of ε_N that is larger than 50%, Tb^{3+} containing films display the highest value of tensile strength. Apparently, this reinforcement effect imparted by metallo-supramolecular interactions can be readily tuned by the stoichiometric ratio of the three metal ions (Fig. S20, ESI†). For instance, the 33:33:33 sample gave a very good comprehensive performance, as shown in Fig. 2 and Table 1.

Rheological properties of the metallo-supramolecular polymers

To further understand the correlation between the dynamic nature of the metallo-supramolecular interactions and the corresponding self-healing properties, rheological tests were performed on films containing different types of metal ions. The master curves (reference temperature: 25 °C) of the three samples (100:0:0, 0:100:0 and 0:0:100) are shown in Fig. 3a, which help to give insight into the structure of these metallo-supramolecular materials in the linear viscoelasticity region. The storage modulus G' and the loss modulus G'' which represent a measure of the elastic response and a measure of the viscous response, respectively, are plotted against the normalized frequency ωa_T *via* time–temperature superposition under small oscillatory shear amplitude ε_0, where a_T is the horizontal shifting factor. Both moduli are in the same order of magnitude and have moderate frequency dependence with a slope of 0.5 on the log–log plot for all three samples (dashed line in Fig. 3a). This 0.5 power law exponent is an intermediate state between the terminal response ($G' \propto \omega^2$, $G'' \propto \omega^1$) of viscoelastic materials and the plateau response ($G' \propto \omega^0$) of well developed network formations and is often observed at the gelation point during a sol–gel transition (incipient gel) according to the percolation theory and numerous experiments on various crosslinking systems.[53,54] This suggests that our bulk films can be classified as weakly crosslinked dynamic materials. It is worthwhile to note that G' is obviously higher than G'' in Tb^{3+} containing films, while they are nearly the same in the Zn^{2+} and Eu^{3+} containing materials. Moreover, concerning the slope at very low ωa_T, in Tb^{3+} containing films both moduli start to deviate from the 0.5 power law dependence towards a plateau response. The above two features reflect the slower dynamics and more elastic response of the Tb^{3+} containing films over the other two materials. In addition, the absolute values of both moduli are in the order of $Zn^{2+} > Tb^{3+} > Eu^{3+}$, which is consistent with the stress response at small strain (Table 1 and Fig. S19†). The dynamic shear viscosity η^* as a function of normalized frequency ωa_T is shown in Fig. 3b. Obviously, the terminal zone was not reached. Thus it is impossible to obtain the exact values of the zero shear viscosity η_0, but they should be well above 100 kPa s. Judging from Fig. 3b at low frequency, the Zn^{2+} containing sample should exhibit clearly the largest value of η_0 over the other two at 25 °C, which is consistent with the previous report by Rowan *et al.*[55] Strain sweep tests were performed on all samples and typical curves of Tb^{3+} containing films are shown in Fig. 3c. As can be seen, a crossover of G' and G'' occurs when a critical strain is reached. As the strain is increased, G' is significantly lowered, indicating the effective crosslinking points formed by metal–BTP complexes were continuously broken and the corresponding transient network was rapidly destroyed by the strong shear stress once the strain exceeds the linear viscoelasticity region. The temperature sensitivity of these films can be learnt from the master curve shifting factors a_T (Fig. 3d). The Eu^{3+} and Tb^{3+} containing samples have almost the same values of a_T in all three

Table 1 Tensile modulus, strength, fracture strain and toughness of films containing different metal ions as well as their mixture

Sample	Tensile modulus (kPa)	Strength (kPa)	Fracture strain (%)	Toughness (kPa)
0:0:0	3.7 ± 3.4	11 ± 1	1700 ± 325	151 ± 50
100:0:0	227 ± 18	64 ± 8	1300 ± 200	726 ± 175
0:100:0	154 ± 12	161 ± 22	1800 ± 120	1765 ± 260
0:0:100	179 ± 13	223 ± 44	1000 ± 75	1222 ± 260
33:33:33	187 ± 18	242 ± 64	1400 ± 390	1921 ± 290

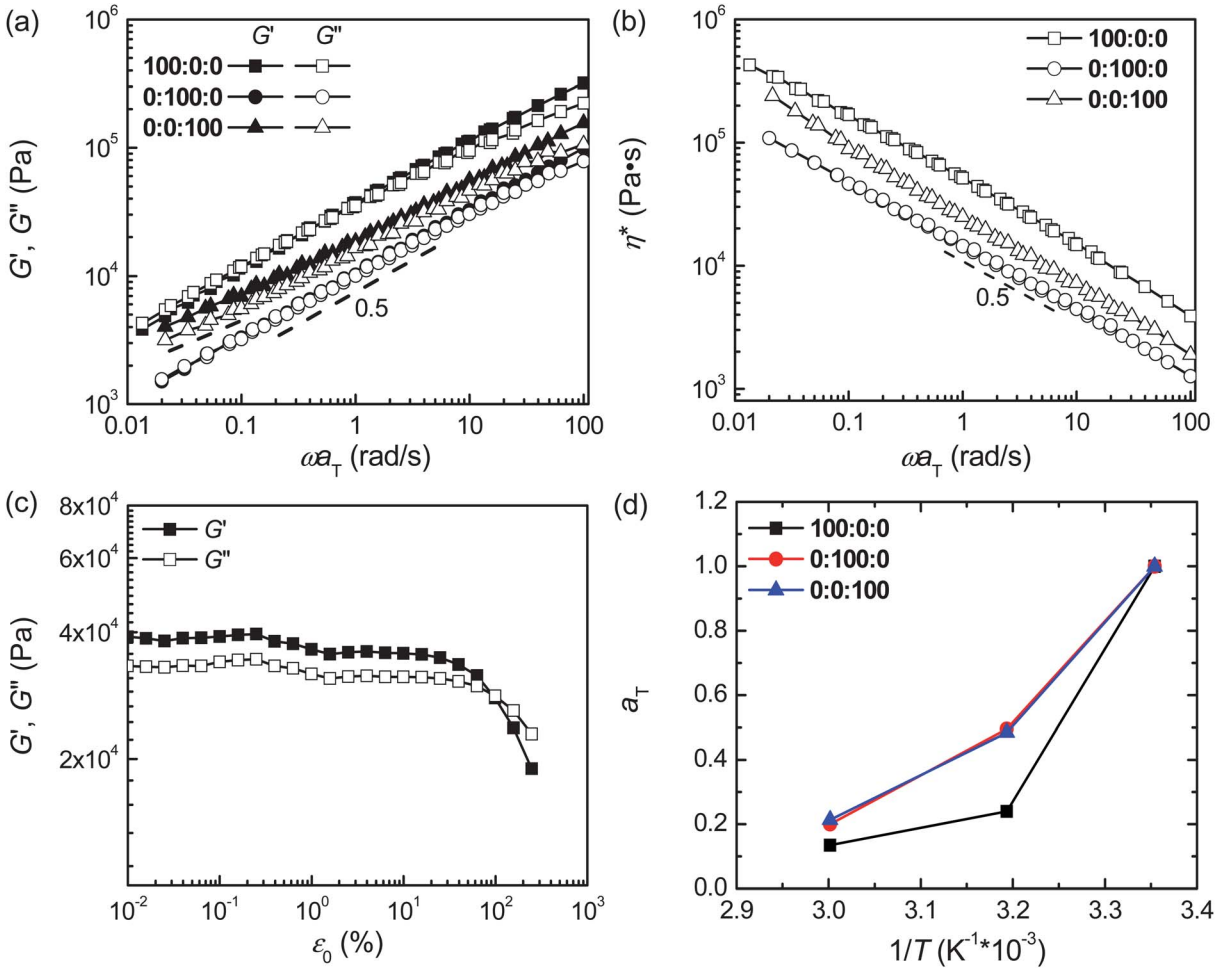

Fig. 3 Rheological tests of the metallo-supramolecular films. (a) Master curves of G' and G'' as a function of normalized frequency ωa_T obtained from time–temperature superposition (reference temperature 25 °C). The legend indicates different types of metal ions. (b) Dynamic shear viscosity η^* as a function of ωa_T. The dashed line indicates the power law exponent. (c) Strain sweep test of a Tb^{3+} containing film at 60 °C with ω = 20 rad s^{-1}. (d) Horizontal shifting factor a_T of a series of films. The relatively smaller values of Zn^{2+} containing films suggest they are more sensitive to temperature.

temperatures examined, while the Zn^{2+} containing films exhibit the strongest temperature sensitivity, presumably due to the microphase separation (*vide infra*).

Microscopic structures of metallo-supramolecular polymers

To gain further insight into the mechanical and rheological properties of the metal ion containing films, the solid state structures of these materials were investigated by small angle X-ray scattering (SAXS), as well as wide angle X-ray diffraction (WXRD). Fig. 4a shows the 1D scattering patterns as a function of the magnitude of the scattering vector q. At the low q region, a shoulder peak (indicated by solid arrows) can be identified at q_1 = 0.50 nm^{-1} (average domain spacing d_1 = 13 nm) in Eu^{3+} containing films (0:100:0), while this value is 0.40 nm^{-1} (corresponding d_1 = 16 nm) in Tb^{3+} containing films (0:0:100), which indicates weak microphase separation of the Eu^{3+}:BTP and Tb^{3+}:BTP complexes with the soft PTHF segments. Further heating up to 80 °C did not efface this q_1 peak (Fig. 4b for 0:0:100 and Fig. S21 in ESI† for 100:0:0 and 0:100:0), implying that the phase-separated structures were thermostable up to 80 °C. This is also the reason to perform the self-healing test on bulk materials at 60 °C (*vide infra*) since the microscopic structures are similar to those at room temperature, but the kinetics can be greatly accelerated. In all the samples containing metal ions, a second peak is recognized at q_2 = 5.34 nm^{-1} (dashed arrow in Fig. 4a), which corresponds to a spacing of 1.2 nm and may be assigned to the metal-to-metal distance in aggregates composed of loosely packed metal–BTP complexes.[56] The q_2 peak was also confirmed by the WAXD tests, as shown in Fig. S22 (ESI).† All three samples studied (100:0:0, 0:100:0 and 0:0:100) show a peak at 2θ of around 7.0–7.5°, consistent with the q_2 peak in the SAXS tests. The broad peaks at 2θ = 22° are probably the amorphous halo. Since Zn^{2+} has a different coordinating number and valence from those of Eu^{3+} and Tb^{3+}, different crosslinking density, chain branching, ionic cluster formation[57] and microphase separation of the different metal–ligand complexes can be expected, leading to the differences in mechanical and rheological properties. In the Zn^{2+} containing films (100:0:0), there was the highest density of crosslinkers of

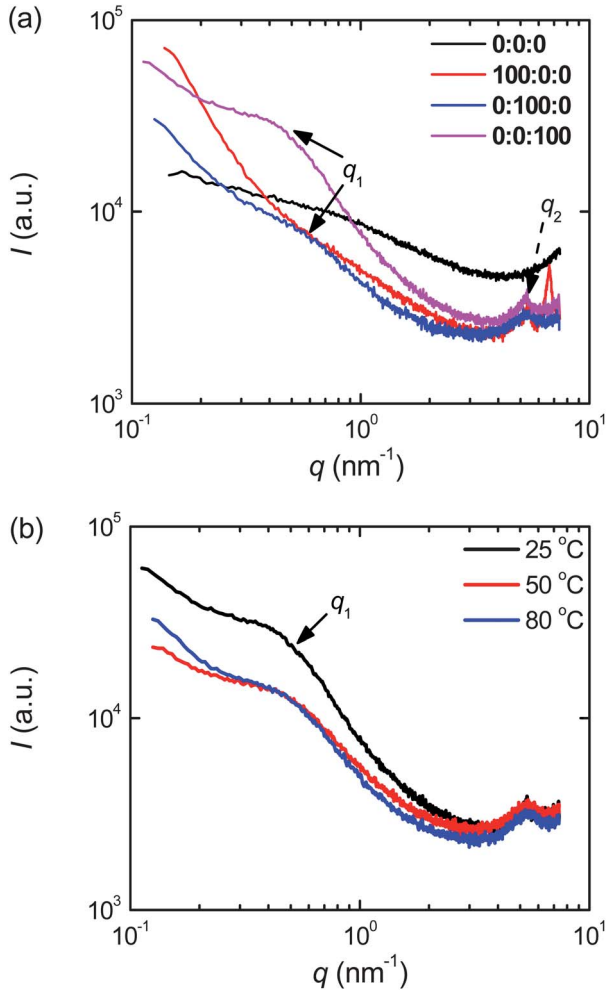

Fig. 4 Scattering intensity I (arbitrary unit) as a function of scattering vector q. (a) The control sample 0:0:0 and the samples containing various types of metal ions: Zn^{2+} (100:0:0), Eu^{3+} (0:100:0) and Tb^{3+} (0:0:100). The solid arrows indicate the primary Bragg peaks q_1 associated with microphase separation, while the dashed arrow marks the second peak q_2; (b) the Tb^{3+} containing films were subjected to heating at different temperatures, as indicated in the legend.

metal–ligand complexes, whereas the chain branching was the lowest and microphase separation could barely be discerned. Therefore, chain entanglement is expected to play an important role in the mechanical properties of the 100:0:0 film. On the other hand, thermostable ionic clusters and phase separated hard phases are most likely absent in 100:0:0, consequently the strongest temperature sensitivity was observed.

Self-healing properties of the metallo-supramolecular polymers and gels

In the first set of experiments, we adopted rheological analyses on the three bulk materials (100:0:0, 0:100:0 and 0:0:100). After the frequency sweep tests demonstrated in Fig. 3a, films were subjected to strain sweep tests at $\omega = 20$ rad s^{-1} to certain oscillatory amplitudes ε_0 (usually between 100% and 1000% depending on the type of metal ion) until G' fell to nearly half of its original value (Fig. 3c and S23†). The healing ability of the films was then immediately monitored by time sweep tests using $\omega = 20$ rad s^{-1} and $\varepsilon_0 = 1\%$ to avoid the effects of shear stress on the self-healing process. The time interval between the strain sweep tests and the time sweep tests was about 10 s. As shown in Fig. 5, the G' values at the beginning of the time sweep tests had already recovered remarkably and soon reached their original values (indicated by the dashed lines) within 20 min for all the samples studied.

The time required to achieve full recovery of the storage modulus G', as well as the corresponding dynamic shear viscosity η^* of the pristine materials at $\omega = 20$ rad s^{-1}, are shown in Table 2 for the three films containing the different metal ions. The initial healing efficiency of all the samples is well above 80%, which again reflects the dynamic nature of the metallo-supramolecular interactions. Nevertheless, the healing rates of the samples significantly depended on the type of metal ions coordinated with the BTP ligands. While the Eu^{3+} containing film (0:100:0) healed within 140 s, the Zn^{2+} (100:0:0) and Tb^{3+} (0:0:100) containing film took about 1180 s and 800 s to reach complete healing, respectively. Given the fact that the dynamic viscosity η^* of the pristine materials at testing conditions ($\omega = 20$ rad s^{-1} and $\varepsilon_0 = 1\%$) is in an order of $Zn^{2+} > Tb^{3+} > Eu^{3+}$, a strong correlation between the healing time and the viscosity of the sample was discovered.

Self-healing generally involves the diffusion of the polymer chains across the wounded interfaces and the reformation of the metal–BTP complexes and/or their aggregates.[58] Therefore, the healing is highly correlated with the binding constant and/or aggregation of the metal–BTP complexes, as well as the diffusion rate of the polymer chains. As there was no phase separation found in the Zn^{2+} containing films (100:0:0) (Fig. 4a), the longest healing time in this material may originate from the lowest coordinating number, the highest binding constant (lowest dynamics of metal–BTP complex) and the lowest chain diffusion rate among the three. Although Zn^{2+} forms kinetically

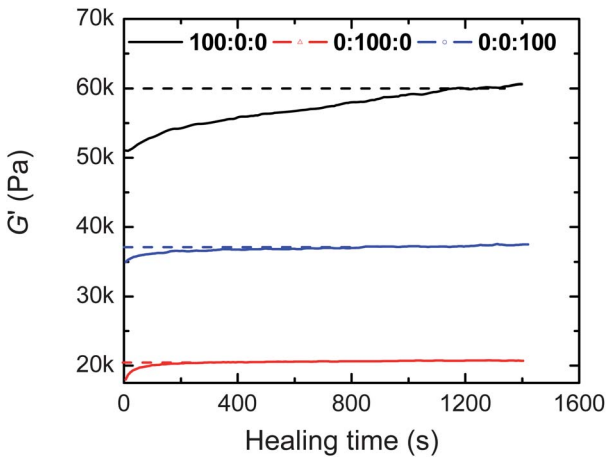

Fig. 5 Recovery of the storage modulus G' measured by time sweep tests at $\omega = 20$ rad s^{-1} and $\varepsilon_0 = 1\%$ under 60 °C immediately after strain sweep tests for the Zn^{2+} (100:0:0), Eu^{3+} (0:100:0) and Tb^{3+} (0:0:100) containing films. The initial moduli are indicated by the dashed lines.

Table 2 The time to achieve full recovery of the storage modulus and the corresponding dynamic viscosity of pristine films made from different metal ions

Samples	Dynamic viscosity η^* at $\omega = 20$ rad s^{-1} (Pa s)	Time to achieve full recovery of G' (s)
Zn^{2+} (100:0:0)	60 000	1180
Eu^{3+} (0:100:0)	20 000	140
Tb^{3+} (0:0:100)	37 000	800

labile complexes with ligands, the binding constants of Zn^{2+} with various ligands have been found to be higher than those of lanthanide ions.[46,59] In addition, as a result of the smaller coordination number of Zn^{2+} to BTP (1 : 2), chain extension in Zn^{2+} containing films is more favourable over chain branching and the effective molecular weight of the assembled ligand macromolecules increases, which will result in more entanglements and higher viscosity. Indeed, it is confirmed by the experimental observation of the highest Young's modulus in tensile tests (Table 1) as well as the largest viscosity in rheological tests (Fig. 3b and Table 2) in Zn^{2+} containing films. A similar phenomenon has also been well documented by Rowan *et al.*[55] The highest viscosity of the Zn^{2+} containing samples significantly hampered the dynamics of the polymer chains from diffusing towards the damaged region and drastically delayed the rate of self-healing.

Although there was phase separation for the Eu^{3+} and Tb^{3+} containing materials (0:100:0 and 0:0:100), the phase separation is weak and the aggregates are expected to be very labile to mechanical force. As the binding of Eu^{3+} and Tb^{3+} with BTP is weaker than that of Zn^{2+}, the complexes are expected to be more dynamic.[50] Therefore, Eu^{3+} and Tb^{3+} containing materials (0:100:0 and 0:0:100) exhibit faster healing rates. Due to the well known effect of lanthanide contraction,[60] Eu^{3+} has a larger radius than Tb^{3+} and presumably exhibits a lower binding constant with BTP than Tb^{3+}. In fact, Martell and Smith have listed the binding constant of Tb^{3+} and Eu^{3+} with all amino acids and Tb^{3+} always has higher binding constant values than Eu^{3+}.[61] As a consequence, superior mechanical strengths and longer healing times were found in Tb^{3+} containing material (0:0:100) over those for 0:100:0. Collectively, the results from the tensile, rheological and self-healing tests of the bulk metallo-supramolecular films were found to be consistent.

In a final demonstration of the importance of metallo-supramolecular interactions in preserving the mechanical properties and in activating the self-healing properties of the materials, another self-healing experiment was conducted. Three dry films (100:0:0, 0:100:0 and 0:0:100) were swollen in toluene to form organic gels (Fig. 6a). The gels were then inspected under UV radiation (254 nm). The BTP ligands can absorb the UV light and transfer the energy to a nearby lanthanide ion, which is then able to emit characteristic metal-centered luminescence (see Fig. S24†). This is the so called "antenna effect".[62] In our system, the colours were blue for 100:0:0, red for 0:100:0 and green for 0:0:100. Therefore, the different gel blocks can be distinguished solely by their

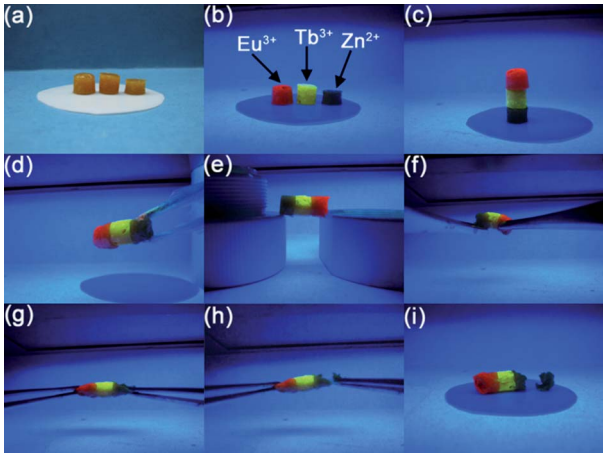

Fig. 6 Self-healing of the metallo-supramolecular gels. (a) Gels containing different metal ions (from left to right are 0:100:0, 0:0:100 and 100:0:0) swollen in toluene; (b) fluorescent image of the three gels under UV light (254 nm); (c) gels were stacked up before self-healing; (d and e) the stacked gels were subjected to self-healing under a saturated toluene atmosphere for 1 h; (f) to (i) the healed gel was then subjected to bending and stretching until fracture.

fluorescent colours, without the use of dye (Fig. 6b). The gels were then stacked up and the jointed gels were then kept under saturated toluene atmosphere for varied times (Fig. 6c). After just 1 h, the jointed gels turned into an integrated one and could hold themselves with different gestures without breaking at the joints (Fig. 6d and e), indicating that healing occurred without any external stimuli (the UV light was turned off during the self-healing process unless taking images, so the photothermal conversion can be neglected). After 20 h, the integrated gel was shown to exhibit very good mechanical properties, as it could be subjected to deformations, such as bending (Fig. 6f) and stretching (Fig. 6g), without breaking at the joints. It is clearly seen in Fig. 6h and i that fracture occurred in the vicinity of the tweezers where the stress concentrated. This examination on the self-healing of gels clearly demonstrates the dynamic nature of metallo-supramolecular interactions and their ability to drive the miscibility and self-healing of the gels and bulk polymers. It should be noted that the three gel blocks were prepared at different times. Therefore, the self-healing of the metallo-supramolecular polymers is almost independent of the waiting time after damage. The metallo-supramolecular gels with one single metal ion exhibited a similar self-healing behaviour (ESI†).

Conclusions

By using CuAAC and thiol–ene double "click" reactions, ligand macromolecules carrying multiple BTP ligand units onto the main chain can be readily prepared. The use of the thiol–ene reaction has many advantages over other reactions. The incorporation of metal ions into the ligand macromolecules resulted in the formation of transient networks crosslinked by supramolecular interactions by forming metal–BTP complexes and sometimes their aggregates as a consequence of microphase

separation. Rheological tests proved that the bulk films were typical weakly crosslinked materials. By selection of the metal–ligand combination and tuning the stoichiometric ratio of metal to ligand, the mechanical properties of the bulk films can be readily tuned. Owing to the dynamic nature of the metallo-supramolecular interactions, the materials were also imparted with the advantage of fast and effective self-healing. We envisage that the CuAAC and thiol–ene "click" reactions can be used in a wide range of responsive and self-healing materials.

Experimental

Materials

Solvents and chemicals were purchased from Sinopharm, Sigma-Aldrich and Aladdin and used without further purification unless otherwise indicated. Toluene, dichloromethane (CH_2Cl_2), dimethyl formamide (DMF), and diisopropylamine (DIPA) were distilled under N_2 over CaH_2, and tetrahydrofuran (THF) over Na, prior to use.

Synthesis and characterization

Synthesis of the BTP ligand. The detailed procedure can be found in the ESI† and the characterization of all the intermediate substances are listed in the ESI Fig. S1 to S5.† Briefly, bis-propene functionalized BTP ligand was prepared *via* CuAAC click reaction of 2,6-diethynyl pyridine and 3-azidoprop-1-ene.

Synthesis of the ligand macromolecule. To a 25 mL quartz flask containing 5 mL chloroform was charged 1.0 g (0.5 mmol, 1.0 equiv.) bis-thiol functionalized PTHF (see ESI†), 0.1 g photo catalyst 2,2-dimethoxy-2-phenylacetophenone and 0.147 g (0.5 mmol, 1.0 equiv.) bis-propene functionalized BTP ligand. The mixture was exposed to UV radiation (200 W cm^{-2}) for 1.5 h. The crude product was then purified by dialysis to afford the ligand macromolecule (0.7 g, 70% yield). ^{1}H NMR ($CDCl_3$, 400 MHz): δ (ppm) = 8.07 (1H, d, J = 8.0 Hz, C_{Ar}–*H*), 7.92 (1H, d, J = 8.0 Hz, C_{Ar}–*H*), 7.52 (2H, s, C_{Ar}–*H*), 7.41 (1H, t, J = 8.0 Hz, C_{Ar}–*H*), 4.10–4.14 (4H, m, COOCH_2), 3.56–3.58 (4H, m, NCH_2), 3.37–3.45 ((4n + 4)H, m, OCH_2), 2.60–3.0 (16H, m, SCH_2), 1.54–1.68 ((4n + 12)H, m, CH_2). ^{13}C NMR (400 MHz, $CDCl_3$): δ (ppm) = 171.8 (2m*n*C), 136.9 (mC), 132.8 (mC), 131.0 (mC), 130.0 (mC), 128.9.0 (mC), 138.5 (mC), 128.1 (mC), 126.9 (mC), 120.5 (mC), 70.6 (2m(n + 1)C), 64.6 (2 mC), 52.9 (2 mC); 50.0 (7 mC), 32.2 (2m), 26.5 (2m(n + 2)C). The molecular weights and polydispersity index estimated from GPC are M_n = 12 kg mol^{-1}, M_w = 22 kg mol^{-1} and PDI = 1.83.

Film and gel preparation. The ligand macromolecule (0.5 g) was first dissolved in chloroform (2 mL) in customized Teflon molds (3 cm in diameter). Then prescribed amounts of solutions of $Zn(OTf)_2$ (0.06 mol L^{-1}), $Tb(OTf)_3$ (0.04 mol L^{-1}) and $Eu(OTf)_3$ (0.04 mol L^{-1}) in methyl cyanide were slowly dropped into the stirring polymer solutions. The mixture was debubbled by centrifugation and slowly dried under room temperature for 48 h. The leftover solvent was further removed by vacuum for another 12 h and clean films were peeled off from the Teflon molds. The dried films were selectively reswollen with chloroform to form organic gels for self-healing studies.

Stress–strain response. Mechanical curves were obtained on an Instron machine (3343) with a 100 N load cell. Rectangular samples 3 to 4 mm wide and about 0.5 mm thick were gripped onto the clamps and stretched under a strain rate of 0.1 s^{-1}, roughly 0.3 to 0.4 mm s^{-1} of the crosshead velocity. Data is presented in terms of nominal stress $\sigma_N = F/S_0$ (F is the force and S_0 is the area of the unstretched sample) as a function of nominal strain $\varepsilon_N = (L - L_0)/L_0$ (L_0 and L are the distance between the clamps before and after stretching).

Small angle X-ray scattering (SAXS). SAXS measurements were carried out on an Anton Paar SAXSess mc^2 platform using a slit collimation (slit dimensions: 20 × 0.3 mm^2). The scattering vector is defined as $q = 4\pi/\lambda \sin(\theta)$, where λ is the wavelength of the X-ray beam (0.1542 nm) and 2θ is the scattering angle. The sample-to-detector length was 260 mm calibrated by a Silver Behenate standard (q = 1.076 nm^{-1}). The scattering intensities were collected at three temperatures: 25 °C, 50 °C and 80 °C for all of the samples. At each temperature, samples were first equilibrated for 10 min followed by an exposure of 15 min. The 1D scattering intensity was automatically desmeared by the commercial software SAXSquadrant.

Self-healing test. Cylindrical shaped dry films (100:0:0, 0:100:0 and 0:0:100) were first swollen in toluene to form organic gels (250 mg mol^{-1}). Then the gel samples were stacked up on a clean Teflon sheet and kept under saturated toluene atmosphere to allow self-healing for different times ranging from 0 to 20 h. The integrated gel was then subjected to bending and stretching by tweezers to test the result of self-healing. Images were taken under UV radiation (254 nm) to demonstrate the self-healing properties of the metallo-supramolecular polymers at the polymer–polymer interface.

Rheological test. ARES-G2 (TA Instruments) was utilized with an 8 mm parallel plate setup. Films were first loaded under 40 °C at 0.3 N force and allowed 10 min equilibration to remove any strain history and to ensure good contact with the plates. Then the testing temperature was changed to the desired values (25 °C, 40 °C and 60 °C). The typical gap value was between 0.6 and 0.8 mm and automatically adjusted by the instrument during the measurements. Frequency sweep tests were performed at each temperature in the range of 0.1 to 100 rad s^{-1} with an oscillatory amplitude ε_0 = 1% that was inside the linear viscoelasticity region from preliminary experiments. After completing the frequency sweep at 60 °C, samples were subjected to strain sweep tests at the same temperature with a frequency ω = 20 rad s^{-1} until the loss modulus G'' was higher than the storage modulus G' and G' fell to about half of its original value, followed immediately by a time sweep test at the same temperature to monitor the recovery of G' *versus* time with ω = 20 rad s^{-1} and ε_0 = 1%.

Acknowledgements

This work was supported by Natural Science Foundation of China (no. 21074103), the Fundamental Research Funds for the Central Universities (no. 2010121018), Scientific Research Foundation for Returned Scholars and NFFTBS (no. J1210014).

The authors appreciate the help from the TA Instrument Co. Shanghai Branch for the rheological test.

Notes and references

1 S. D. Bergman and F. Wudl, *J. Mater. Chem.*, 2008, **18**, 41–62.
2 D. Y. Wu, S. Meure and D. Solomon, *Prog. Polym. Sci.*, 2008, **33**, 479–522.
3 J. L. Mynar and T. Aida, *Nature*, 2008, **451**, 895–896.
4 E. B. Murphy and F. Wudl, *Prog. Polym. Sci.*, 2010, **35**, 223–251.
5 N. K. Guimard, K. K. Oehlenschlaeger, J. Zhou, S. Hilf, F. G. Schmidt and C. Barner-Kowollik, *Macromol. Chem. Phys.*, 2012, **213**, 131–143.
6 J. A. Syrett, C. R. Becer and D. M. Haddleton, *Polym. Chem.*, 2010, **1**, 978–987.
7 E. V. Skorb and D. V. Andreeva, *Polym. Chem.*, 2013, **4**, 4834.
8 M. Q. Zhang and M. Z. Rong, *Polym. Chem.*, 2013, **4**, 4878.
9 L. R. Hart, J. L. Harries, B. W. Greenland, H. M. Colquhoun and W. Hayes, *Polym. Chem.*, 2013, **4**, 4860.
10 S. R. White, N. R. Sottos, P. H. Geubelle, J. S. Moore, M. R. Kessler, S. R. Sriram, E. N. Brown and S. Viswanathan, *Nature*, 2001, **409**, 794–797.
11 R. S. Trask, G. J. Williams and I. P. Bond, *J. R. Soc. Interface*, 2007, **4**, 363–371.
12 M. M. Caruso, B. J. Blaiszik, S. R. White, N. R. Sottos and J. S. Moore, *Adv. Funct. Mater.*, 2008, **18**, 1898–1904.
13 K. S. Toohey, N. R. Sottos, J. A. Lewis, J. S. Moore and S. R. White, *Nat. Mater.*, 2007, **6**, 581–585.
14 K. S. Toohey, C. J. Hansen, J. A. Lewis, S. R. White and N. R. Sottos, *Adv. Funct. Mater.*, 2009, **19**, 1399–1405.
15 C. C. Corten and M. W. Urban, *Adv. Mater.*, 2009, **21**, 5011–5015.
16 N. Kwok and H. T. Hahn, *J. Compos. Mater.*, 2007, **41**, 1635–1654.
17 J.-H. Park and P. V. Braun, *Adv. Mater.*, 2010, **22**, 496–499.
18 Q. Wei, J. Wang, X. Shen, X. A. Zhang, J. Z. Sun, A. Qin and B. Z. Tang, *Sci. Rep.*, 2013, **3**, 1093.
19 M. D. Hager, P. Greil, C. Leyens, S. van der Zwaag and U. S. Schubert, *Adv. Mater.*, 2010, **22**, 5424–5430.
20 F. Herbst, D. Döhler, P. Michael and W. H. Binder, *Macromol. Rapid Commun.*, 2013, **34**, 197–203.
21 R. J. Wojtecki, M. A. Meador and S. J. Rowan, *Nat. Mater.*, 2011, **10**, 14–27.
22 X. X. Chen, M. A. Dam, K. Ono, A. Mal, H. B. Shen, S. R. Nutt, K. Sheran and F. Wudl, *Science*, 2002, **295**, 1698–1702.
23 B. J. Adzima, C. J. Kloxin and C. N. Bowman, *Adv. Mater.*, 2010, **22**, 2784–2787.
24 P. Reutenauer, E. Buhler, P. J. Boul, S. J. Candau and J. M. Lehn, *Chem.–Eur. J.*, 2009, **15**, 1893–1900.
25 Y.-L. Liu and T.-W. Chuo, *Polym. Chem.*, 2013, **4**, 2194–2205.
26 C. M. Chung, Y. S. Roh, S. Y. Cho and J. G. Kim, *Chem. Mater.*, 2004, **16**, 3982–3984.
27 H. Otsuka, K. Aotani, Y. Higaki, Y. Amamoto and A. Takahara, *Macromolecules*, 2007, **40**, 1429–1434.
28 G. Deng, C. Tang, F. Li, H. Jiang and Y. Chen, *Macromolecules*, 2010, **43**, 1191–1194.
29 J. Canadell, H. Goossens and B. Klumperman, *Macromolecules*, 2011, **44**, 2536–2541.
30 H. Otsuka, S. Nagano, Y. Kobashi, T. Maeda and A. Takahara, *Chem. Commun.*, 2010, **46**, 1150–1152.
31 Y. Amamoto, J. Kamada, H. Otsuka, A. Takahara and K. Matyjaszewski, *Angew. Chem., Int. Ed.*, 2011, **50**, 1660–1663.
32 Y.-X. Lu, F. Tournilhac, L. Leibler and Z. Guan, *J. Am. Chem. Soc.*, 2012, **134**, 8424–8427.
33 Y.-X. Lu and Z. Guan, *J. Am. Chem. Soc.*, 2012, **134**, 14226–14231.
34 F. Herbst, S. Seiffert and W. H. Binder, *Polym. Chem.*, 2012, **3**, 3084–3092.
35 P. Cordier, F. Tournilhac, C. Soulie-Ziakovic and L. Leibler, *Nature*, 2008, **451**, 977–980.
36 A. Vidyasagar, K. Handore and K. M. Sureshan, *Angew. Chem., Int. Ed.*, 2011, **50**, 8021–8024.
37 G. Jiang, C. Liu, X. Liu, G. Zhang, M. Yang and F. Liu, *Macromol. Mater. Eng.*, 2009, **294**, 815–820.
38 S. Burattini, B. W. Greenland, D. H. Merino, W. Weng, J. Seppala, H. M. Colquhoun, W. Hayes, M. E. Mackay, I. W. Hamley and S. J. Rowan, *J. Am. Chem. Soc.*, 2010, **132**, 12051–12058.
39 S. Burattini, B. W. Greenland, W. Hayes, M. E. Mackay, S. J. Rowan and H. M. Colquhoun, *Chem. Mater.*, 2011, **23**, 6–8.
40 S. Burattini, H. M. Colquhoun, J. D. Fox, D. Friedmann, B. W. Greenland, P. J. F. Harris, W. Hayes, M. E. Mackay and S. J. Rowan, *Chem. Commun.*, 2009, 6717–6719.
41 Q. Wang, J. L. Mynar, M. Yoshida, E. Lee, M. Lee, K. Okuro, K. Kinbara and T. Aida, *Nature*, 2010, **463**, 339–343.
42 A. B. South and L. A. Lyon, *Angew. Chem., Int. Ed.*, 2010, **49**, 767–771.
43 X. Wang, F. Liu, X. Zheng and J. Sun, *Angew. Chem., Int. Ed.*, 2011, **50**, 11378–11381.
44 W. Weng, Z. Li, A. M. Jamieson and S. J. Rowan, *Soft Matter*, 2009, **5**, 4647–4657.
45 W. Weng, Z. Li, A. M. Jamieson and S. J. Rowan, *Macromolecules*, 2009, **42**, 236–246.
46 W. Weng, J. B. Beck, A. M. Jamieson and S. J. Rowan, *J. Am. Chem. Soc.*, 2006, **128**, 11663–11672.
47 M. Burnworth, L. Tang, J. R. Kumpfer, A. J. Duncan, F. L. Beyer, G. L. Fiore, S. J. Rowan and C. Weder, *Nature*, 2011, **472**, 334–337.
48 M. Zhang, D. Xu, X. Yan, J. Chen, S. Dong, B. Zheng and F. Huang, *Angew. Chem., Int. Ed.*, 2012, **51**, 7011–7015.
49 U. Mansfeld, A. Winter, M. D. Hager, R. Hoogenboom, W. Guenther and U. S. Schubert, *Polym. Chem.*, 2013, **4**, 113–123.
50 Y. Chen, A. M. Kushner, G. A. Williams and Z. Guan, *Nat. Chem.*, 2012, **4**, 467–472.
51 J. Yuan, X. Fang, L. Zhang, G. Hong, Y. Lin, Q. Zheng, Y. Xu, Y. Ruan, W. Weng, H. Xia and G. Chen, *J. Mater. Chem.*, 2012, **22**, 11515–11522.
52 M. J. Kade, D. J. Burke and C. J. Hawker, *J. Polym. Sci., Part A: Polym. Chem.*, 2010, **48**, 743–750.
53 H. H. Winter and F. Chambon, *J. Rheol.*, 1986, **30**, 367–382.

54 H. H. Winter and M. Mours, in *Neutron Spin Echo Spectroscopy Viscoelasticity Rheology*, 1997, vol. 134, pp. 165–234.
55 J. R. Kumpfer, J. J. Wie, J. P. Swanson, F. L. Beyer, M. E. Mackay and S. J. Rowan, *Macromolecules*, 2012, **45**, 473–480.
56 J. R. Kumpfer, J. Jin and S. J. Rowan, *J. Mater. Chem.*, 2010, **20**, 145–151.
57 S. Bode, L. Zedler, F. H. Schacher, B. Dietzek, M. Schmitt, J. Popp, M. D. Hager and U. S. Schubert, *Adv. Mater.*, 2013, **25**, 1634–1638.
58 J. D. Fox and S. J. Rowan, *Macromolecules*, 2009, **42**, 6823–6835.
59 Y. Zhao, J. B. Beck, S. J. Rowan and A. M. Jamieson, *Macromolecules*, 2004, **37**, 3529–3531.
60 C. E. Housecroft and A. G. Sharpe, *Inorganic Chemistry*, Prentice Hall, 2nd edn, 2004, pp. 536, 649, 743.
61 A. E. Martell and R. M. Smith, *Critical Stability Constants*, Plenum Press, 1977, pp. 71–420.
62 N. Sabbatini, M. Guardigli and J.-M. Lehn, *Coord. Chem. Rev.*, 1993, **123**, 201–228.